Scalable NMR spectroscopy with semiconductor chips

Dongwan Ha[a], Jeffrey Paulsen[b], Nan Sun[c], Yi-Qiao Song[b], and Donhee Ham[a,1]

[a]School of Engineering and Applied Sciences, Harvard University, Cambridge, MA 02138; [b]Schlumberger-Doll Research Center, Cambridge, MA 02139; and [c]Electrical and Computer Engineering, The University of Texas at Austin, Austin, TX 78712

Edited by Adriaan Bax, National Institutes of Health, Bethesda, MD, and approved July 8, 2014 (received for review February 1, 2014)

State-of-the-art NMR spectrometers using superconducting magnets have enabled, with their ultrafine spectral resolution, the determination of the structure of large molecules such as proteins, which is one of the most profound applications of modern NMR spectroscopy. Many chemical and biotechnological applications, however, involve only small-to-medium size molecules, for which the ultrafine resolution of the bulky, expensive, and high-maintenance NMR spectrometers is not required. For these applications, there is a critical need for portable, affordable, and low-maintenance NMR spectrometers to enable in-field, on-demand, or online applications (e.g., quality control, chemical reaction monitoring) and co-use of NMR with other analytical methods (e.g., chromatography, electrophoresis). As a critical step toward NMR spectrometer miniaturization, small permanent magnets with high field homogeneity have been developed. In contrast, NMR spectrometer electronics capable of modern multidimensional spectroscopy have thus far remained bulky. Complementing the magnet miniaturization, here we integrate the NMR spectrometer electronics into 4-mm^2 silicon chips. Furthermore, we perform various multidimensional NMR spectroscopies by operating these spectrometer electronics chips together with a compact permanent magnet. This combination of the spectrometer-electronics-on-a-chip with a permanent magnet represents a useful step toward miniaturization of the overall NMR spectrometer into a portable platform.

NMR spectroscopy has been celebrated for its ability to probe molecular structures and dynamics with the atomic resolution (1–9). State-of-the-art NMR spectrometers use large superconducting magnets, whose high and uniform magnetic fields lead to the fine spectral resolution necessary for interrogating large molecules such as proteins. In fact, the structural study of large molecules is one of the most profound applications of modern NMR spectroscopy.

However, the spectral resolution of the bulky, expensive, and high-maintenance NMR spectrometers is not necessary for a broad array of studies involving small-to-medium size molecules in chemistry, chemical engineering, and biotechnology (10, 11). In this case, portable, affordable, and low-maintenance NMR spectrometers built with a permanent magnet can make the benefits of NMR spectroscopy more broadly available and enable new applications. Bulky superconducting systems have to be permanently placed in dedicated laboratories, but portable systems can enable in-field, on-demand, or online applications such as quality control and chemical reaction monitoring (4), and can greatly facilitate co-use of NMR spectroscopy with other analytical methods such as liquid chromatography (12) and capillary electrophoresis (13). Thus, much effort has been devoted to miniaturizing NMR spectrometers, leading to the critical development of small permanent magnets with high field homogeneity (10, 14, 15).

Complementing this advance in magnet miniaturization, here we integrate the spectrometer electronics—which is another essential, and traditionally bulky, component of the NMR spectrometer—into a 4-mm^2 silicon chip (Fig. 1). Moreover, to demonstrate the overall system miniaturization for portability, we operate these chips with a compact 0.51-T permanent magnet (Fig. 1), performing various two-dimensional (2D) spectroscopies—correlation spectroscopy (COSY), *J*-resolved spectroscopy, and heteronuclear single/multiple-quantum coherence (HSQC/HMQC) spectroscopy—as well as one-dimensional (1D) spectroscopy and relaxometry. Various organic, biological, and drug compound molecules are used as demonstrational samples.

Although semiconductor technology and NMR science have remained largely orthogonal, a few foundational works reported silicon chips realizing some aspects of NMR electronics before the present study (16–20). Despite the vision and tour de force design, however, none of these earlier chips explored modern multidimensional spectroscopy. In refs. 16, 17, the chip design focus was not on spectroscopy, but on relaxometry, with a dedicated integrated Carr–Purcell–Meiboom–Gill (CPMG) pulse sequencer to achieve overall relaxometry system miniaturization with permanent magnets. The chips in refs. 18–20 performed spectroscopy but limited to 1D and with external pulse sequencers (and with external transmitters in refs. 18, 19), and they were operated with superconducting magnets, and thus were far from portable. Significantly building upon these prior works, we integrate at a large scale a radio-frequency (RF) transmitter, an RF receiver, and an arbitrary pulse sequencer into our spectrometer electronics chip so that it can perform a far more diverse set of NMR experiments, including 2D spectroscopy, in an integrated manner. In addition, our overall system is the first portable NMR spectroscopy platform to our knowledge that combines permanent magnets and spectrometer electronics chips. In view of this, the present work is a step forward in utilizing semiconductor technology for portable NMR spectroscopy.

In addition to these main contributions, our portable system incorporates two other features to cope with ambient temperature variations, which are relevant to portable applications. First, the spectrometer electronics chips are designed to operate over a wide temperature range (room temperature to 165 °C). Second, a signal-processing method based on statistical estimation/inference—which

Significance

The strong application-driven need for portable NMR spectrometers has led to development of spectroscopy-grade permanent magnets. In contrast, NMR spectrometer electronics capable of modern multidimensional spectroscopy remain bulky. Here, we report on 4-mm^2 silicon spectrometer electronics chips, and perform various multidimensional NMR spectroscopies by using these chips with a permanent magnet. This combination of semiconductor technology and advanced permanent magnet technology is a step toward portable NMR spectrometers, which can enable in-field, on-demand, or online applications and facilitate co-use of NMR with other analytical methods. Besides the portable application, the spectrometer electronics chips with their cost/size economy can improve other NMR technologies—whether with permanent or superconducting magnet—such as multi-channel spectroscopy, phased-array imaging, microfluidic microscopy, and parallel, high-throughput spectroscopy.

Author contributions: D. Ha, Y.-Q.S., and D. Ham designed research; D. Ha, J.P., N.S., Y.-Q.S., and D. Ham performed research; D. Ha, J.P., N.S., Y.-Q.S., and D. Ham analyzed data; D. Ha designed integrated circuits; D. Ham oversaw research; and D. Ha and D. Ham wrote the paper.

The authors declare no conflict of interest.

This article is a PNAS Direct Submission.

[1]To whom correspondence should be addressed. Email: donhee@seas.harvard.edu.

This article contains supporting information online at www.pnas.org/lookup/suppl/doi:10.1073/pnas.1402015111/-/DCSupplemental.

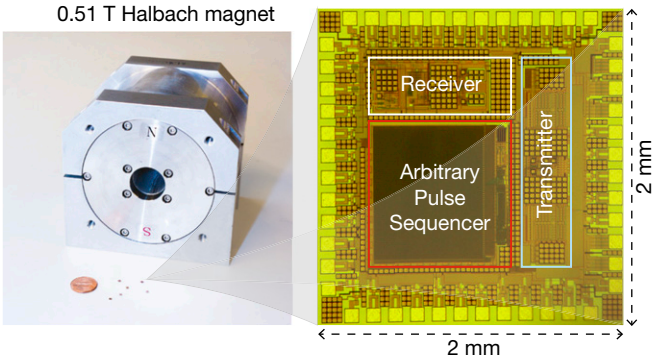

Fig. 1. NMR spectrometer combining silicon spectrometer electronics chips and a 0.51-T NdFeB permanent magnet (W × D × H: 12.6 × 11.7 × 11.9 cm^3; weight: 7.3 kg; Neomax Co.).

does not require isolated reference peaks as in the reference deconvolution technique (21)—calibrates out the effect of the permanent magnet's field drift caused by environmental temperature fluctuations. This software-domain method, as an addition to the arsenal of various magnetic field fluctuation calibration techniques, may help reduce the need for physical thermal regulation that adds power consumption and extra hardware, the avoidance of which, if possible, is desired for portable applications.

Results

Magnet and Coil. All spectroscopy experiments in this work (see Figs. 3–6) use a solenoidal coil (axial length: 1 mm) around a capillary sample tube (i.d.: 1 mm) with an effective sample volume of 0.8 μL, and a compact 0.51-T NdFeB permanent magnet with a 0.13-ppm field inhomogeneity achieved with a six-direction electrical shimming (*Materials and Methods*). The inductance L_c and resistance R_c of the coil are 173 nH and 0.75 Ω, respectively. The ^{1}H Larmor frequency, f_0, is 21.8 MHz with the magnet, and the quality factor of the coil at f_0 is $Q = 2\pi f_0 L_c/R_c \sim 31.5$.

NMR Spectrometer Electronics Chips. The integrated spectrometer electronics chip consists of three main parts, an RF receiver, an RF transmitter, and an arbitrary pulse sequencer (Fig. 2). The RF receiver amplifies the voltage signal across the coil induced by nuclear spin precessions using a front-end low-noise amplifier (*SI Appendix*, section S1), and down converts the amplified signal into two phase-sensitive audio-frequency signals using mixers driven by quadrature local oscillators. Spectral information is extracted by taking the Fourier transform of these audio-frequency signals. The overall receiver voltage gain is tunable from 34 to 100 dB.

Because the inherently weak spin precession signal is further reduced to ~1 μV in our case due to the small sample and low magnetic field, maximizing receiver sensitivity—i.e., minimizing the degradation of the signal-to-noise ratio (SNR) by receiver noise—is a critical task. First, we minimize the input-referred noise of the receiver to a measured value of $N_r^2 = 0.82^2$ $(nV)^2/Hz$ at 300 K (Fig. 2*B* and *SI Appendix*, section S1), which translates to an effective noise resistance of $R_r = 40.6$ Ω. However, this step alone, albeit crucial, is not sufficient, because the source noise $N_c^2 = 0.11^2$ $(nV)^2/Hz$ inside the coil due to $R_c = 0.75$ Ω is still far smaller than N_r^2 and thus, the SNR would be greatly degraded by the dominant receiver noise. Hence our second step is to add an off-chip tuning capacitor C_c in parallel to the coil so that L_c and C_c resonate at f_0 (Fig. 2); the resonator quality factor is still Q = 31.5, as the capacitor loss is negligible. Due to this resonance, the effective coil voltage (for both noise and signal) seen by the receiver at frequency f_0 is approximately Q times larger than the actual voltage inside the coil; thus the effective coil noise, $Q^2N_c^2$, is ~18 times larger than the receiver noise, N_r^2 (or, the effective coil noise resistance Q^2R_c = 744 Ω is ~18 times larger than R_r = 40.6 Ω). Therefore, the receiver noise reduces the source SNR only by 5%, leading to a receiver noise figure—the ratio of SNR at the receiver input to that at the receiver output, $(Q^2N_c^2 + N_r^2)/Q^2N_c^2 = (Q^2R_c + R_r)/Q^2R_c$—of only 0.23 dB. This fares well, if not better, with commercial spectrometer electronics (cf. Magritek Kea: preamp noise figure < 1.5 dB). This resonant noise figure reduction technique is widely used in traditional spectrometer electronics, but is made simpler and more effective in our case, as the coil and spectrometer electronics chip are not intervened by a transmission line (16, 17).

The RF transmitter to excite nuclear spins and manipulate their motions consists of a multiphase generator and a power amplifier (Fig. 2). An RF excitation signal first goes through a multiphase generator (*SI Appendix*, section S1; also for its experimental demonstration, see Fig. 2*A*), which is based on a time-delay line consisting of 32 equal delay segments. The total delay through the entire line is tightly regulated at one RF period, or a phase of 2π, where this regulation is accomplished by negative feedback set around the delay line. The output of the

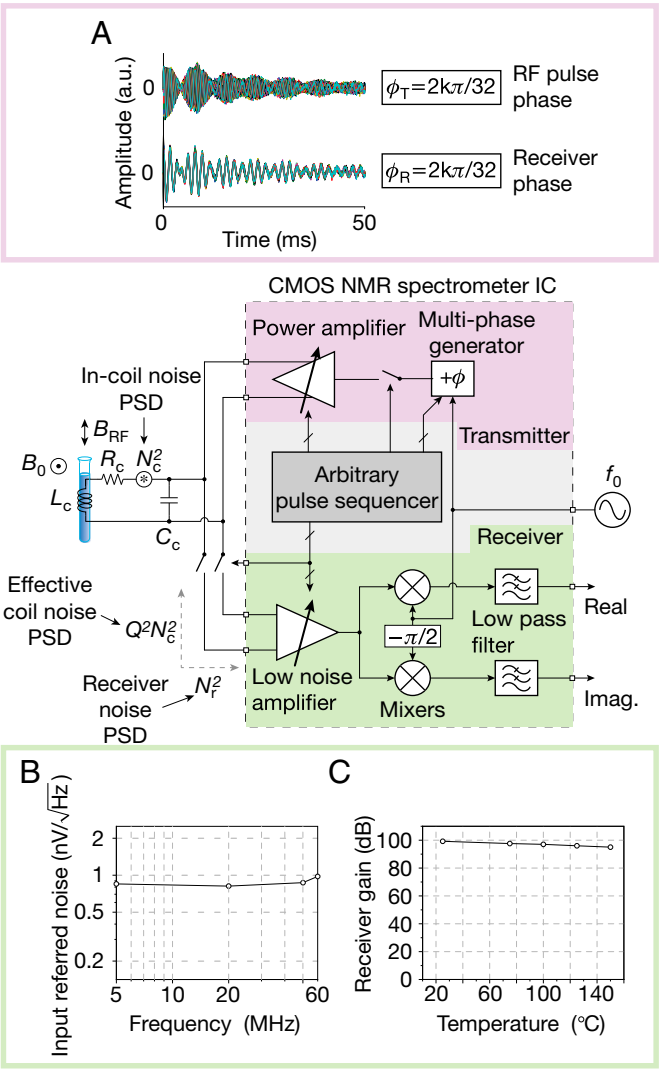

Fig. 2. Spectrometer electronics chip architecture and measurements. (*A*) Free-induction decay (FID) experiments with ethylbenzene demonstrate multiphase generation; 32 FID signals excited by π/2 pulses with 32 different RF phases (*Upper*) are aligned (*Lower*), after shifting each signal by its respective excitation phase. These particular experiments were done before the magnet shimming. (*B*) Receiver input referred noise; and (*C*) receiver gain.

multiphase generator is an RF signal tapped off at one of the 32 nodes of the line; thus, the RF phase can be chosen among 32 values between 0 and 2π with a resolution of π/16. This RF signal with a particularly chosen phase subsequently drives the power amplifier (*SI Appendix*, section S1), which injects an RF power of 23.7 mW into the coil, sustaining an RF current amplitude of ∼251 mA in the coil. This produces an RF magnetic field amplitude of 9.4 G, corresponding to a π/2-pulse duration of 6.3-μs for protons (^{1}H).

The input signal path to the power amplifier can be turned on and off to create an RF pulse and a delay, and the RF phase of the pulse has been already selected among the 32 values by the preceding multiphase generator. By such control of the power amplifier and multiphase generator, we produce a broad variety of pulse sequences. This control of the power amplifier and multiphase generator is coordinated by the arbitrary pulse sequencer (Fig. 2 and *SI Appendix*, section S1), which consists of a digital signal processor and a 4,096-bit memory. The memory stores a set of digital codes that represent a specific pulse sequence, and can be refreshed through a standard serial peripheral interface. The sequencer runs with a 16-MHz clock with a time resolution of 62.5 ns, which is ∼100 times smaller than the π/2-pulse duration of 6.3-μs. The sequencer also controls the RF receiver, by activating it during a signal acquisition and by blanking it during an RF pulse transmission. In this way, the arbitrary pulse sequencer works as the control center that manages the entire operation of the spectrometer electronics chip. In summary, our spectrometer electronics chip can produce a variety of RF pulse sequences, enabling the broad palette of multidimensional NMR spectroscopy, which will be demonstrated in full shortly. Incidentally, for portable applications where temperature can vary, our chip is designed with temperature-compensated features so that it can operate from room temperature to over 165 °C (*SI Appendix*, section S1). For instance, the measured receiver gain is varied only by 4 dB from 25 to 150 °C (Fig. 2*C*).

In this spectrometer electronics chip, we have focused on integrating the RF transceivers and arbitrary pulse sequencer that are the performance bottlenecks, and the RF frequency source (local oscillator) and analog-to-digital converter (ADC) are not integrated. An Agilent 81150A function generator is used as the RF source. Its measured phase noise for $f_0 = 21.8$ MHz is −116.7 dBc/Hz at 10-kHz offset, which translates to a phase diffusion coefficient (22, 23) of 4.2×10^{-3} rad^2 Hz. This causes a phase error of only 0.09 rad or 0.014 RF cycle after 1 s of 21.8×10^6 RF oscillations. Thus, the phase noise has no appreciable impact at all on any of our experiments. An external ADC (LT1407A) with a 14-bit resolution was used with a 20-kHz sampling rate for all our spectroscopy experiments. As seen, because the performance criteria for the RF frequency source and ADC are not stringent, they can be integrated into the spectrometer electronics chip in the future development stage.

Multidimensional NMR Spectroscopy. Our system with the setup of Fig. 3*A* reproduces the well-known 1D ^{1}H NMR spectra of various small molecules (Fig. 3 *B*–*H*). For example, chemical shifts of the OH, CH_2, and CH_3 groups in ethanol (CH_3CH_2OH, 99.5%) and those of the residual HDO solvent, CH and CH_3 groups in L-alanine ($C_3H_7NO_2$, 1.5 M dissolved in D_2O) all manifest correctly from left to right. The ethanol and L-alanine spectra also correctly exhibit *J*-coupled peaks. For aspirin, L-serine, and D-(+)-glucose, some peaks within 0.13 ppm were not fully resolved, limited by the inhomogeneity of the permanent magnet used.

Fig. 4*B* shows the *J*-resolved 2D ^{1}H spectra of ethanol and L-alanine. For ethanol (Fig. 4*B*, *Left*), the *J* coupling between the CH_3 and CH_2 groups via three successive single bonds manifests as ∼7-Hz vertical peak splittings at each of the CH_3 and CH_2 chemical shifts that horizontally line up. The CH_3 group

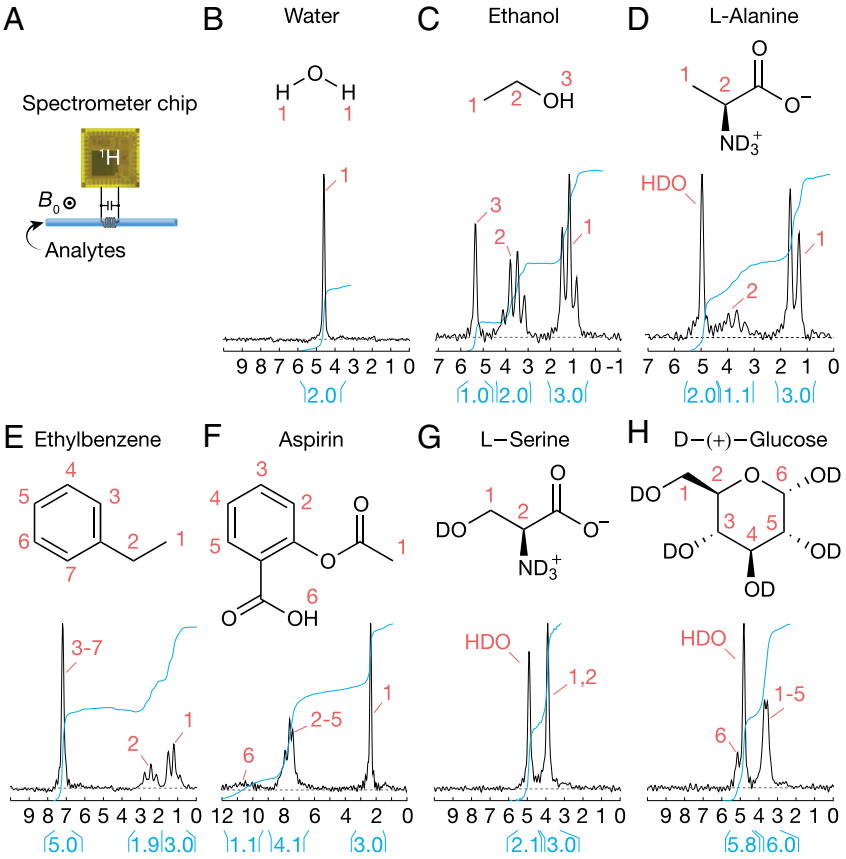

Fig. 3. One-dimensional ^{1}H NMR spectroscopy. (*A*) Setup. (*B*–*H*) The 1D spectra for deionized tap water (1 scan), ethanol (1 scan), L-alanine (64 scans), ethylbenzene (1 scan), aspirin (64 scans), L-serine (64 scans), and D-(+)-glucose (64 scans). L-alanine, L-serine, and D-(+)-glucose are dissolved in D_2O (1.5 M). Aspirin is dissolved in DMSO-d6 (1.5 M).

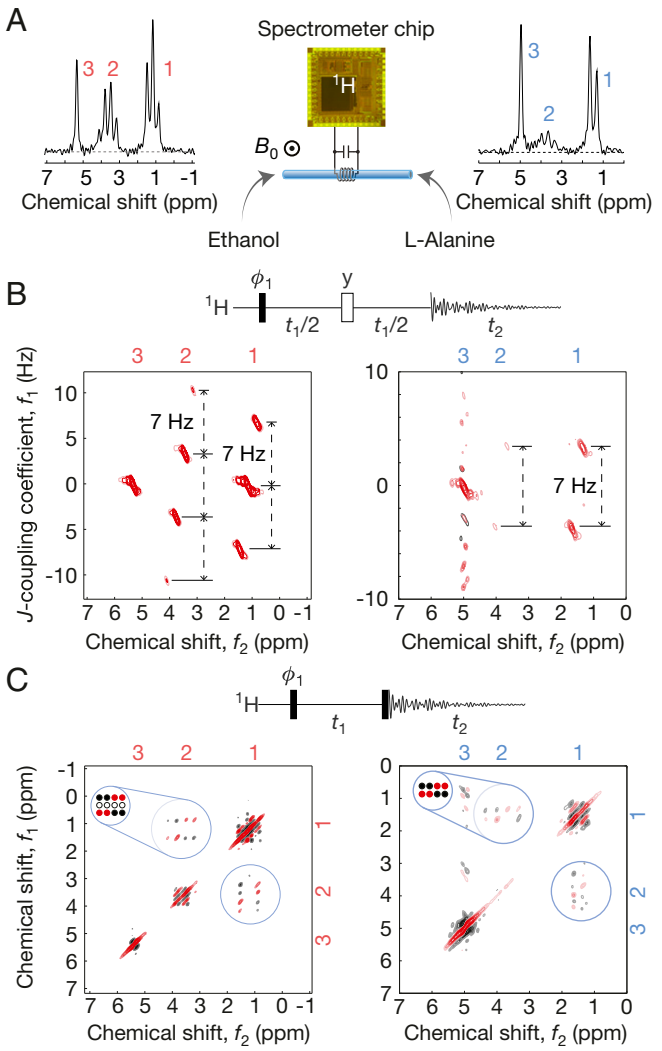

Fig. 4. Two-dimensional ^{1}H NMR spectroscopy. (*A*) Setup; 1D spectra of ethanol and L-alanine, identical to Fig. 3 *C* and *D*. (*B*) *J*-resolved spectra of ethanol (*Left*) and L-alanine (*Right*); each takes 15 min to obtain (84 scans with a single scan/wait time of 11 s). In the pulse sequence, black (white) bar signifies a $\pi/2$ (π) pulse. Quadrature detection in the f_1 domain is done by additional phase cycle with ϕ_1 shifted by $\pi/2$ (41). (*C*) COSY spectra of ethanol (*Left*) and L-alanine (*Right*); each takes 73 min to acquire (400 scans with a single scan/wait time of 11 s).

interacting with the ^{1}H spin triplet of the CH_2 group exhibits three vertical peaks; the CH_2 group interacting with the quadruplet energy states of the ^{1}H spins of the CH_3 group show four vertical peaks. The *J* coupling between the CH_3 and CH groups in L-alanine also correctly yields ~7-Hz splittings (Fig. 4*B*, *Right*), and the two outermost vertical peaks of the CH group, which appear weak in the 1D spectrum (Fig. 3*D*), fall below the threshold chosen for this 2D contour map.

Another demonstration of 2D ^{1}H NMR is for the COSY spectra of ethanol and L-alanine (Fig. 4*C*). The off-diagonal cross-peak multiplets unambiguously identify the above-discussed *J* couplings. These cross-peak multiplet patterns for both molecules agree with the theoretical predictions depicted around the top left corner of their respective 2D spectra—the red (black) filled circles signify positive (negative) absorption line shapes; empty circles represent no peaks—except obfuscation of certain peaks in the measured L-alanine data. This loss of some fine features is due to low signal-to-noise ratio, which can be improved by using a magnet with a higher field or by increasing sample volume, if the field is more homogenous.

We also perform two-channel heteronuclear (^{1}H/^{13}C) 2D NMR by operating two chips synchronously (Fig. 5*A*). In particular, we perform HSQC and HMQC on ^{13}C-enriched methanol ($^{13}CH_3OH$, 98% purity, 99% enriched) to identify the ^{1}H—^{13}C single-bond coupling. The ^{1}H channel, used for both excitation and detection, consists of a spectrometer electronics chip and a solenoidal coil around the capillary tube. The excitation-only ^{13}C channel consists of a second chip and a separate ^{13}C coil placed underneath the capillary. The orthogonal orientation of the two coils minimizes mutual interactions. Although one doubly tuned coil (24) can be used, we use the two coils for simplicity of their design. The 1D ^{1}H spectrum without activating the ^{13}C channel (Fig. 5*B*) shows two large peaks with a 140-Hz splitting originating from the ^{1}H—^{13}C *J* coupling (the third smaller peak is from the OH group). HSQC and HMQC (Fig. 5 *C* and *D*) use both ^{13}C and ^{1}H channels for excitation and magnetization transfer, and only the ^{1}H channel is used for detection. In each of the resulting spectra, the two peaks separated by 140 Hz along the ^{1}H spectrum appear at the same ^{13}C chemical shift, unequivocally identifying the ^{13}C—^{1}H single-bond coupling. As the OH proton is uncoupled to a carbon, its signal vanishes in the 2D spectra.

Calibration of Magnetic Field Fluctuation. Because the permanent magnet's field significantly varies with the ambient temperature

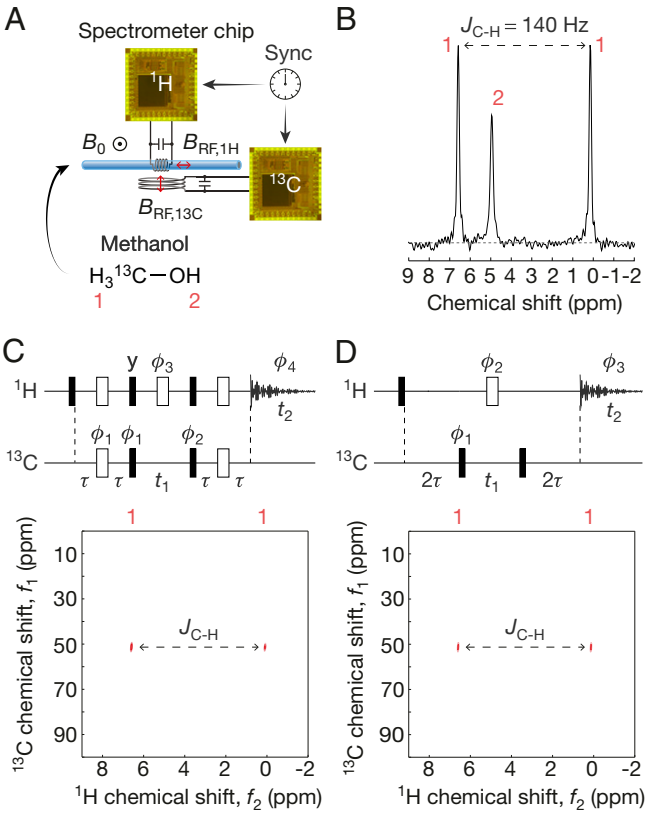

Fig. 5. Two-dimensional heteronuclear spectroscopy with methanol. (*A*) Setup. (*B*) ^{1}H-only 1D spectrum. (*C*) HSQC spectrum. A four-phase cycling to select the particular coherence pathway uses $\phi_1 \in \{0,\pi,0,\pi\}$, $\phi_2 \in \{0,0,\pi,\pi\}$, and $\phi_3 \in \{0,\pi,\pi,0\}$. HSQC spectrum takes 17 min to obtain (168 scans including phase cycling with a single scan/wait time of 6 s). (*D*) HMQC spectrum. An eight-phase cycling to select the particular coherence pathway uses $\phi_1 \in \{0,\pi,0,\pi,0,\pi,0,\pi\}$, $\phi_2 \in \{0,0,\pi/2,\ \pi/2,\pi,\pi,3\pi/2,3\pi/2\}$, and $\phi_3 \in \{0,\pi,\pi,0,0,\pi,\pi,0\}$. HMQC spectrum takes 34 min to acquire (336 scans including phase cycling with a single scan/wait time of 6 s). For *C* and *D*, the ^{13}C $\pi/2$-pulse duration is obtained separately (*Materials and Methods*), and $\tau = 1/(4J_{C-H})$.

(−1,200 ppm/K), the Larmor frequency exhibits appreciable temporal fluctuations, thus distorting NMR spectra. This effect is especially pronounced in long-term multiple-scan experiments, such as 2D spectroscopy (e.g., Larmor frequency fluctuates up to ∼800 Hz in the ethanol COSY experiment). In fact, these field fluctuations have been recognized as one significant obstacle toward portable NMR spectroscopy (11, 25).

We devise a signal-processing method to calibrate out the fluctuation effect (*SI Appendix*, section S2). All 1D and 2D spectra in Figs. 3–5 are indeed the outcome of this method applied to raw data. Our method is distinct from the reference deconvolution (21) that extracts the fluctuation information by comparing measured and theoretical shapes of well-defined, isolated reference peaks from extra materials, such as tetramethylsilane or $^{13}C/^{2}H$ (26, 27). By contrast, instead of relying on known reference peaks from extra materials, our method statistically infers the fluctuation information from the very data from the analyte under test—via statistical distance and entropy minimization—treating the field fluctuation as a slow random process (*SI Appendix*, section S2). Although this method can be applied only when the field fluctuation is slow compared with a single scan time, it adds to the repertoire of existing calibration techniques, and worked effectively in all our spectroscopy experiments, as such slow fluctuation is not an impractical assumption; see Fig. 6 for an example calibration result (full details of our method and additional data are found in *SI Appendix*, section S2). Our method may be useful in on-demand/portable situations where using the reference materials/peaks as in the reference deconvolution is cumbersome or impractical.

It should be noted that a very well-stabilized magnet with physical thermal regulation would yield better spectra than the unregulated magnet with calibration techniques, and such thermal regulation is necessary when the SNR is too poor to apply calibration techniques. However, when calibration techniques are applicable, avoiding the thermal regulation—which requires extra hardware and increases the power consumption—but using such a software-domain calibration technique could be desirable, particularly for portable applications.

NMR Relaxometry. Because the arbitrary pulse sequence generator can readily produce a long sequence of a multitude of repeated RF pulses, our chip can also perform 1D and 2D relaxation experiments (28), such as CPMG experiments to measure spin–spin relaxation time, T_2, in the presence of static field inhomogeneity. We demonstrate this in the context of petroleum exploration to understand the properties of the complex fluids in the earth formations (29–31), for it is a significant venue for ^{1}H NMR relaxometry (32, 33). Specifically, we use CPMG to measure T_2 of a medium-weight crude oil (from Texas; room temperature viscosity 25.5 cP) at room temperature and at 150 °C that emulates the deep subsurface and demonstrates the high-temperature performance of the spectrometer electronics chip. This experiment uses a different solenoidal coil (axial length: 9 mm), a larger glass capillary (i.d.: 2.42 mm; sample volume: 41 μL), and a 0.3-T cylindrical SmCo magnet (diameter: 8 cm; height: 3.9 cm; weight: ∼0.9 kg; Metrolab). This magnet is capable of 150 °C operation due to its high Curie temperature (∼800 °C), and has a field inhomogeneity of ∼100 ppm over the sample volume. The entire setup is placed in a temperature-controlled chamber (Fig. 7*A*). The power amplifier of our spectrometer electronics chip can drive this 50 times larger sample volume of 41 μL, transmitting a 37.6 mW of RF power into the coil. An RF current with an amplitude of 388 mA is sustained in the coil, with the corresponding π/2-pulse duration being 15 μs. The transmitter is further capable of transmitting up to 182 mW of RF power into the coil (*SI Appendix*, section S1).

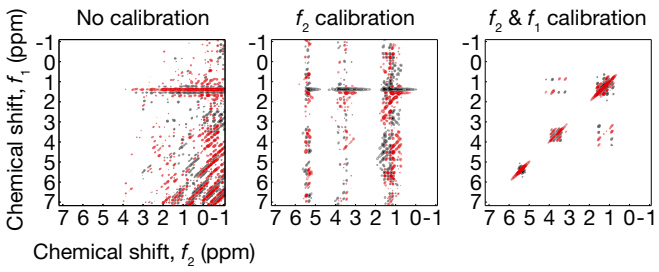

Fig. 6. Raw, f_2-calibrated, and f_2- and f_1-calibrated COSY ethanol spectrum; the final one is identical to Fig. 4*C*, *Left*.

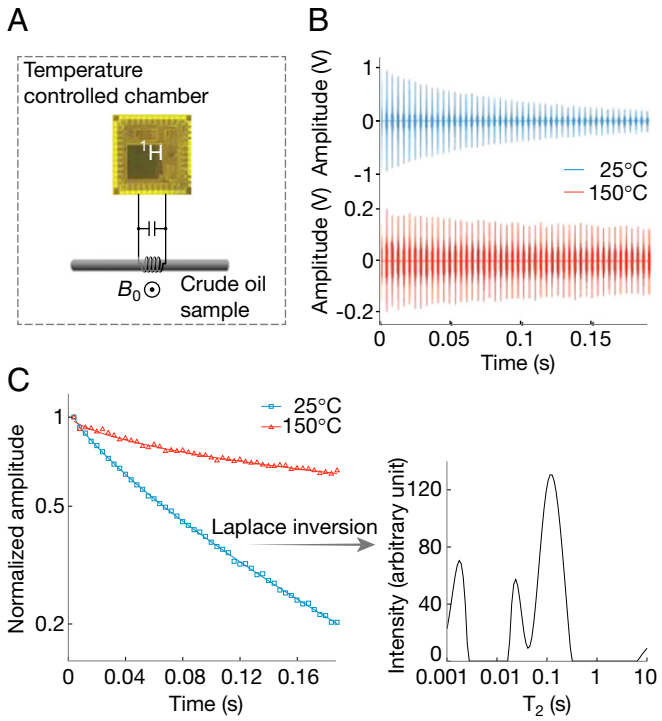

Fig. 7. ^{1}H NMR relaxometry for a crude oil sample. (*A*) Setup. (*B*) CPMG echo signal vs. echo time at 25 °C (blue) and 150 °C (red). (*C*, *Left*) Semilog plot of the echo decay at 25 °C (blue) and 150 °C (red). Echo spacing is 4 ms. (*Right*) T_2 spectrum at 25 °C.

The measured spin echoes (Fig. 7*B*) exhibit an overall slower decay (longer T_2) at 150 °C than at 25 °C due to faster molecular motion at the higher temperature (30). Semilog plots of the echo signal at both temperatures (Fig. 7*C*, *Left*) reveal a nonexponential decay, indicating the presence of multiple decay exponents. Laplace inversion of the decays yields broad T_2 spectra (Fig. 7*C*, *Right,* is an example at 25 °C) corresponding to the broad distribution of molecular weights of hydrocarbons in the crude oil (31), where lighter molecules exhibit more rapid thermal motions thus longer T_2. This relaxometry with the spectrometer electronics chip can be used to characterize complex fluid composition at elevated temperatures.

Discussion

The combination of semiconductor technology and permanent magnet we have demonstrated for multidimensional NMR spectroscopy may help accelerate the advance of portable NMR spectroscopy. Such portable systems would enable the application of NMR spectroscopy to situations where large, expensive conventional NMR spectrometers cannot be installed, yet online or on-demand analysis is ideal or necessary. For example, portable systems can be used in an industrial production line to inspect the product quality (34), or on/inside benchtop/hood to facilitate analysis of intermediate/final products and kinetics of chemical reactions (4, 35). In addition, such miniaturized system

may also facilitate, and lower the cost of, multimodal analysis where NMR spectroscopy is combined with and complemented by other analytical methods such as liquid chromatography (12), capillary electrophoresis (13), mass spectrometry, and Fourier transform infrared spectroscopy. The NMR sensitivity of these miniaturized systems can be further enhanced by techniques such as parahydrogen polarization transfer (36).

Besides the portable applications with the overall system miniaturization, the spectrometer electronics chips alone—whether used with a permanent or superconducting magnet—can help improve various other NMR technologies. For instance, such spectrometer electronics chips can greatly simplify the setup and reduce the cost of multichannel experiments (as implied by our HSQC and HMQC experiments), such as multichannel acquisition spectroscopy (27), phased-array applications (37, 38), and multichannel microscopic flow monitoring (2). Furthermore, a cluster of spectrometer electronics chips and microcoils (39) placed within a superconducting magnet bore may enable highly parallel NMR spectroscopy, countering the inherent slowness of individual NMR spectroscopy experiment and enabling the high-throughput paradigm for pharmaceutical screening (3), structural biology (5), and metabolomics/metabonomics (9). In such a parallel experimental scheme with many silicon chips inside the magnet bore, because the materials of the silicon chips have nonzero magnetic susceptibility, their optimal placement with coils and compensation of their magnetic effects will be a critical problem to address to minimize their impact on the field homogeneity.

Materials and Methods

Fabrication and Packaging of the Spectrometer Electronics Chips. We design the chips in complementary metal-oxide-semiconductor (CMOS) 0.18-μm technology and have them fabricated by Taiwan Semiconductor Manufacturing Co. The chips are packaged in 48-pin ceramic leadless chip carriers.

Electrical Shimming of the NdFeB Magnet. Two printed circuit boards, each containing planar loop coils, are placed facing each other inside the NdFeB magnet. The coils are electronically controlled to produce correction field gradients. The coils are patterned in particular shapes (e.g., circular loop) (40) so that they can correct the field in six directions: x, y, xz, yz, z, and $2z^2 - (x^2 + y^2)$. The shimming yields 0.13-ppm FWHM in the 1D spectrum of water (Fig. 3*B*).

Selection of the ^{13}C $\pi/2$-Pulse Duration (Fig. 5). We determine the ^{13}C $\pi/2$-pulse duration by using a variation of the HMQC pulse sequence (Fig. 5*D*) with $t_1 = 0$ and phase cycling of $\phi_1 \in \{0,\pi\}$, $\phi_2 \in \{\pi/2,\pi/2\}$, and $\phi_3 \in \{\pi,0\}$, and by maximizing the amplitude of the resulting ^{1}H signal.

Materials. ^{13}C-enriched methanol is from Cambridge Isotope. All other chemicals are from Sigma Aldrich.

ACKNOWLEDGMENTS. We thank Drs. Soumyajit Mandal and Jeffrey Crank (Schlumberger), Dr. Shaw Huang (Harvard Laukien-Purcell Center), Mr. Jeffrey Abbott (Harvard University), and Drs. Werner Maas, James Kempf, Brian Marquez, and Sridevi Krishnamurthy (Bruker Biospin) for discussions. We thank Schlumberger, Air Force Office of Scientific Research (FA9550-13-1-0211), Office of Naval Research (N00014-13-1-0806), and National Science Foundation (NSF-1254459) for support.

1. Aue WP, Bartholdi E, Ernst RR (1976) Two–dimensional spectroscopy. Application to nuclear magnetic resonance. *J Chem Phys* 64(5):2229–2246.
2. Bajaj VS, Paulsen J, Harel E, Pines A (2010) Zooming in on microscopic flow by remotely detected MRI. *Science* 330(6007):1078–1081.
3. Pellecchia M, Sem DS, Wüthrich K (2002) NMR in drug discovery. *Nat Rev Drug Discov* 1(3):211–219.
4. Wensink H, et al. (2005) Measuring reaction kinetics in a lab-on-a-chip by microcoil NMR. *Lab Chip* 5(3):280–284.
5. Wüthrich K (2003) NMR studies of structure and function of biological macromolecules (Nobel lecture). *Angew Chem Int Ed Engl* 42(29):3340–3363.
6. Baldwin AJ, Kay LE (2009) NMR spectroscopy brings invisible protein states into focus. *Nat Chem Biol* 5(11):808–814.
7. Inomata K, et al. (2009) High-resolution multi-dimensional NMR spectroscopy of proteins in human cells. *Nature* 458(7234):106–109.
8. Sakakibara D, et al. (2009) Protein structure determination in living cells by in-cell NMR spectroscopy. *Nature* 458(7234):102–105.
9. Nicholson JK, Lindon JC (2008) Systems biology: Metabonomics. *Nature* 455(7216): 1054–1056.
10. Danieli E, Perlo J, Blümich B, Casanova F (2010) Small magnets for portable NMR spectrometers. *Angew Chem Int Ed Engl* 49(24):4133–4135.
11. Luy B (2011) Towards portable high-resolution NMR spectroscopy. *Angew Chem Int Ed Engl* 50(2):354–356.
12. Foley DA, et al. (2013) Online NMR and HPLC as a reaction monitoring platform for pharmaceutical process development. *Anal Chem* 85(19):8928–8932.
13. Diekmann J, et al. (2011) Portable microcoil NMR detection coupled to capillary electrophoresis. *Anal Chem* 83(4):1328–1335.
14. McDowell A, Fukushima E (2008) Ultracompact NMR: 1H spectroscopy in a subkilogram magnet. *Appl Magn Reson* 35(1):185–195.
15. Perlo J, Casanova F, Blümich B (2007) Ex situ NMR in highly homogeneous fields: 1H spectroscopy. *Science* 315(5815):1110–1112.
16. Sun N, Liu Y, Lee H, Weissleder R, Ham D (2009) CMOS RF biosensor utilizing nuclear magnetic resonance. *IEEE J Solid-State Circuits* 44(5):1629–1643.
17. Sun N, et al. (2011) Palm NMR and 1-chip NMR. *IEEE J Solid-State Circuits* 46(1): 342–352.
18. Anders J, Chiaramonte G, SanGiorgio P, Boero G (2009) A single-chip array of NMR receivers. *J Magn Reson* 201(2):239–249.
19. Anders J, SanGiorgio P, Boero G (2011) A fully integrated IQ-receiver for NMR microscopy. *J Magn Reson* 209(1):1–7.
20. Kim J, Hammer B, Harjani R (2012) A 5-300MHz CMOS transceiver for multi-nuclear NMR spectroscopy. *IEEE Custom Integr Circ Conf*:1–4.
21. Morris GA, Barjat H, Home TJ (1997) Reference deconvolution methods. *Prog Nucl Mag Res Sp* 31(2):197–257.
22. Ham D, Hajimiri A (2003) Virtual damping and Einstein relation in oscillators. *IEEE J Solid-State Circuits* 38(3):407–418.
23. Li X, Yildirim OO, Zhu W, Ham D (2010) Phase noise of distributed oscillators. *IEEE Trans Microw Theory Tech* 58(8):2105–2117.
24. Cross VR, Hester RK, Waugh JS (1976) Single coil probe with transmission-line tuning for nuclear magnetic double resonance. *Rev Sci Instrum* 47(12):1486–1488.
25. Zalesskiy SS, Danieli E, Blümich B, Ananikov VP (2014) Miniaturization of NMR systems: Desktop spectrometers, microcoil spectroscopy, and "NMR on a chip" for chemistry, biochemistry, and industry. *Chem Rev* 114(11):5641–5694.
26. Iijima T, Takegoshi K (2008) Compensation of effect of field instability by reference deconvolution with phase reconstruction. *J Magn Reson* 191(1):128–134.
27. Kupče E (2013) NMR with multiple receivers. *Top Curr Chem* 335:71–96.
28. Song Y-Q (2013) Magnetic resonance of porous media (MRPM): A perspective. *J Magn Reson* 229:12–24.
29. Song YQ, Ryu S, Sen PN (2000) Determining multiple length scales in rocks. *Nature* 406(6792):178–181.
30. Freed DE (2007) Dependence on chain length of NMR relaxation times in mixtures of alkanes. *J Chem Phys* 126(17):174502.
31. Freed DE, Burcaw L, Song Y-Q (2005) Scaling laws for diffusion coefficients in mixtures of alkanes. *Phys Rev Lett* 94(6):067602.
32. Lee H, Sun E, Ham D, Weissleder R (2008) Chip-NMR biosensor for detection and molecular analysis of cells. *Nat Med* 14(8):869–874.
33. Sun N, et al. (2013) Small NMR biomolecular sensors. *Solid-State Electron* 84:13–21.
34. Linck YG, Killner MHM, Danieli E, Blümich B (2013) Mobile low-field 1H NMR spectroscopy desktop analysis of biodiesel production. *Appl Magn Reson* 44(1-2):41–53.
35. Küster SK, Danieli E, Blümich B, Casanova F (2011) High-resolution NMR spectroscopy under the fume hood. *Phys Chem Chem Phys* 13(29):13172–13176.
36. Colell J, et al. (2013) Fundamental aspects of parahydrogen enhanced low-field nuclear magnetic resonance. *Phys Rev Lett* 110(13):137602.
37. Gruschke OG, et al. (2012) Lab on a chip phased-array MR multi-platform analysis system. *Lab Chip* 12(3):495–502.
38. Wiggins GC, et al. (2009) 96-Channel receive-only head coil for 3 Tesla: Design optimization and evaluation. *Magn Reson Med* 62(3):754–762.
39. Olson DL, Peck TL, Webb AG, Magin RL, Sweedler JV (1995) High-resolution microcoil 1H-NMR for mass-limited, nanoliter-volume samples. *Science* 270(5244):1967–1970.
40. Anderson WA (1961) Electrical current shims for correcting magnetic fields. *Rev Sci Instrum* 32(3):241–250.
41. Keeler J, Neuhaus D (1985) Comparison and evaluation of methods for two-dimensional NMR spectra with absorption-mode lineshapes. *J Magn Reson* 63(3): 454–472.